



# Microscopic deformation mechanism and characteristics of carbonaceous slate during the creep process

Hucheng Yang · Peng Li · Shengrui Su ·  
Jianxun Chen

Received: 5 March 2023 / Accepted: 9 June 2024  
© The Author(s) 2024

**Abstract** Carbonaceous slate exhibits a significant creep deformation that seriously affects the construction and operation of underground projects. To investigate the microstructural changes characteristics and reveal the microscopic deformation mechanism of the carbonaceous slate during the creep process, multiple methods were performed, including the triaxial creep test, SEM and MIP. The following conclusions were drawn: The rock samples underwent three stages during the creep test: microporosity closure at a low-stress level, material densification at an intermediate stress level, and microcracks emerging and expanding to failure at the high stress. The creep deformation was particularly significant in the first and third processes. The lamellar particles are compressed or

bent under stress in parallel and vertical directions, showing the anisotropic properties of deformation. The deformation of the rock sample is related to the angle between the bedding and the orientation of major principal stress, and the effect of the anisotropy decreases with the increased stress level. The sprouting and expansion of microfractures occur at high-stress levels, showing pressure dissolution of mineral particles, migration of very fine particles, and cement damage between lamellar particles. Finally, the horizontal samples formed a combined rupture surface composed of the laminar surface and the fracture surface intersecting it, showing brittle damage, while the vertical samples formed a fracture surface parallel to the laminar surface, showing a ductile damage pattern. Those results could provide the basis for a further understanding of the mechanical properties of carbonaceous slate and the improvement of its creep model and parameters. It was significant for the stability analysis and deformation prediction of engineering structures using numerical simulation.

---

H. Yang  
College of Geology Engineering and Geomatics, Chang'an University, Xi'an 710054, China

H. Yang  
College of Architecture and Engineering, Yan'an University, Yan'an 716000, China

P. Li (✉) · S. Su (✉)  
College of Geology Engineering and Geomatics, Chang'an University, Xi'an 710054, China  
e-mail: lipeng198782@163.com

S. Su  
e-mail: shengruisu@163.com

J. Chen  
School of Highway, Chang'an University, Xi'an 710054, China

## Article highlights

- The deformation and microstructural characteristics of carbonaceous slate during triaxial compression creep were investigated.
- The creep process and deformation mechanism of carbonaceous slate were analyzed from the microscopic perspective.

- The microporosity closure of carbonaceous slate at low-pressure stress levels and the occurrence of pressure dissolution and particle migration in the fracture region at high-stress levels are revealed.

**Keywords** Carbonaceous slate · Microstructure · Pore size distribution · Creep process · Deformation mechanics

## 1 Introduction

Carbonaceous slate is a low-grade metamorphic rock with a pervasive occurrence of foliations, cleavages, beddings, and fractures. As a laminar soft rock, it is characterized by transversely isotropic mechanical behavior, low strength, and large time-dependent deformation under a complex geologic environment. The deformation of soft rock, being extremely large and lasting for a long time, has brought a great challenge to tunnel construction and seriously hindered the development of tunnel projects in western China (Chen et al. 2011; Li et al. 2013). The creep behaviors of rock extensively affect the stability of the surrounding rock and tunnel structure safety. Extensive creep tests have been conducted on soft rocks (Tomanovic 2006; Zhang et al. 2012, 2015a; Hamza et al. 2018). The time-dependent process is critical to accurately predict the strength and deformation in the short and long term due to the safety of the tunnel in construction and operation and its economic importance (Hamza and Stace 2018). Some researchers focused on the time-dependent deformation characteristics of various rocks (Haupt 1991; Maranini and Brignoli 1999; Shao et al. 2003; Gasc-Barbier et al. 2004; Pellet 2006; Sun 2007). The creep curve was divided into three parts: primary or transient creep, secondary or stationary creep, and tertiary creep or creep failure (Scholz 1968; Boukharov et al. 1995; Gunther et al. 2015; Zhang et al. 2020). Extensive macroscopic mechanical studies have been conducted to gain a better understanding of the transversely isotropic behavior of layered rock and found that the deformation and strength differ when the rocks are subjected to different loading directions (Tien et al. 2006; Shi et al. 2016; Wang et al. 2018a). Sone and Zoback (2013) concluded

that more creep deformation in shale rock samples deformed perpendicular than parallel to the bedding plane. At an identical stress state in triaxial creep tests, the axial strain rates of the carbonaceous slate with a bedding plane perpendicular to axial loading were higher than those of the specimens with a bedding plane parallel to axial loading (Wang et al. 2018b). Boukharov et al. (1995) revealed that the properties of a heterogeneous rock depended not only upon the minerals component but upon the structural features of the rocks as well, and those features were the size difference of individual mineral crystals, boundaries between the crystals, pores, and microcracks occurring in and/or between the crystals. The mechanical response of a rock is linked to its mesoscale elements, such as voids, grains, and matrix cracks; the formation and development of fine cracks are significantly time-dependent and directly affect the time-dependent deformation of the rock (Lin and Sun 1993). Zhang and Buscarnera (2017) mentioned that the creep process was controlled by the growth of internal flaws and the delayed fracture of individual particles; numerous microscopic processes at low or high pressures influenced the rate-dependent behavior of granular rocks. The particle strength depends considerably on size, shape, and mineralogy. The macroscopic yield pressure is connected with the grain size and the specific fracture process developing at the grain scale (Zhang et al. 2015b). The main factors affecting creep are groundwater, mineral composition, ground stress, geological structure, and construction disturbance. Sun (2007) believed that the essence of creep was that new filling and arrangement patterns occur continuously between mineral assemblages or between mineral assemblages and other rock components over time. Indeed, grain-scale phenomena can impact the constitutive properties of granular soil, such as yield pressure, plastic compressibility, and frictional resistance; the particle strength depends considerably on factors such as size, shape, and mineralogy (Coop et al. 2004; Brzesowsky et al. 2014). Based on the analysis of laboratory and in-situ experiments, Boukharov (1995) concluded that the creep of brittle rock was an integral manifestation of three modes of rock deformation: elastic strain, plastic strain, and inelastic dilatancy. The carbonaceous slate has remarkable rheological characteristics, displaying obvious viscoelasticity,

and the mechanical behaviors cannot be well explained using linear elastic and isotropic theories (Zhao et al. 2018). Some nonlinear and visco-plastic models were proposed and effectively applied to numerical simulation to describe the theoretical creep stage (Xu et al. 2006; Sterpi and Gioda 2009; Debernardi and Barla 2009; Barla et al. 2012). A series of nonlinear visco-elastic–plastic creep models were established using the Hooke body, Schiffman body, Kelvin body, and nonlinear visco-plastic body (Yang et al. 2014). Barla et al. (2012) used two elastic-visco-plastic constitutive laws implemented in finite-difference and finite-element codes to study the squeezing behavior of tunnels through numerical analysis. The formulations of the mathematical creep models of the rock often display good agreement with the test data. However, they are limited by unclear physical meaning of the parameters of the material, which are determined by the characteristics of the material and obtained by measurements on the samples in the laboratory. Understanding such phenomena requires a comprehensive inspection of deformation characteristics at both macroscopic and particle scales.

Many studies on the macroscopic creep behavior of various rocks and the corresponding constitutive relationship for numerical simulation obtain fruitful results. However, there are fewer studies on the carbonaceous slate, and the creep mechanisms are far from being well understood. Multiple methods were adopted in this study to investigate the creep deformation characteristics of carbonaceous slate and analyze the rules of the axial and radial strain of the horizontal and vertical samples in loading and creep processes combined with the variations of particles and pores structure, revealing the deformation mechanisms. Explanation of the deformation with information on microstructure and porosity characteristics during the triaxial creep tests is scientifically reasonable in explaining creep deformation mechanisms. Hence, it is crucial to familiarize oneself with the time-dependent deformational behaviors of carbonaceous slate from a microscopic view. The studies contribute to a better understanding of the creep mechanisms of carbonaceous slate and provide a better basis for optimization of the constitutive model and related parameters to predict the long-term stability of engineering structures.

## 2 Materials and test apparatus

### 2.1 Samples preparation

The rocks selected for the laboratory experiments were obtained from the Muzhailing highway tunnel at Dingxi City, Gansu province, China. The surrounding rock showed remarkably time-dependent deformation caused by boundary constraint conditions and stress changes in the areas dominated by carbonaceous slate during the tunnel excavation. Representative rock blocks were picked during tunnel excavation, and the samples were cored carefully from selected similar blocks to reduce the disturbance factors that may cause the variation of rock characteristics.

Firstly, four cylindrical specimens with a height of about 100 mm and 50 mm in diameter were cored along the horizontal and vertical bedding planes, called horizontal and vertical samples, respectively. Two specimens of each bedding angle were selected as triaxial creep samples. Then, For the high-resolution studies of very fine-grained phases, six cubes of about  $10\times 10\times 2$  mm samples were ion-polished to obtain a smooth surface for high-resolution imaging and prepared for SEM. Five cubes of about  $10\times 10\times 10$  mm were made for MIP tests. Four rock sections were thin pieces of rock cutting from the different direction of the rock sample. They were then ground into a thickness of about 0.03 mm and attached to the high-purity slides. Those small samples were all made from the residual block material. Finally, the small blocks of the damaged samples from the two kinds of rheological tests were processed into six cubes of about  $10\times 10\times 2$  mm and  $10\times 10\times 10$  mm and prepared for the SEM and MIP tests, respectively.

### 2.2 Test apparatus

The microstructure of carbonaceous slate was first studied. The mineral composition and surface morphology of samples were analyzed from diffraction patterns and high-resolution imaging obtained by environmental scanning electron microscope with energy-dispersive spectroscopy (SEM–EDS) detectors using the quantor 200 (FEI, USA). The resolution is 3.5 nm in high vacuum mode, the magnification is 50–50000 times, and the maximum pixel is  $3584\times 3084$ . Thin section identification was conducted with a petrographic microscope of Axiolab 5

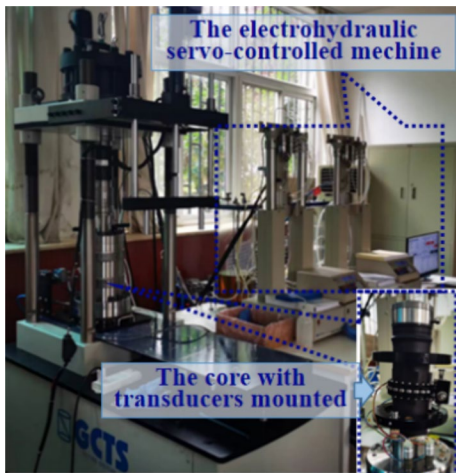


**Fig. 1** Schematic diagram of the creep test device

(ZEISS Germany) to study the microstructure. The instrument used for the MIP test is the MicroActive Autopore Iv 9510, with a mercury drive pressure range of 0.5–33,000 psi and a pore size range of 35  $\mu\text{m}$  to 5 nm to study the pore size and distribution. Then, the creep tests were achieved by the GCTS RTX-1000 testing systems (GCTS USA), seen in Fig. 1, which is a triaxial electrohydraulic servo-controlled testing machine. The system comprises a closed-loop digital servo-controlled rock triaxial test system RTX-1000 and a GCTS data acquisition system. Two linear variable displacement transducers are applied to measure the axial strain, and a chain transducer is employed to measure the radial strain, fixed outside the specimen. The confining stress and deviatoric stress were all applied by the hydraulic pumps. The loading scheme is automatically controlled by a pre-written program, and the pressures are automatically regulated by the computer in the creep process. The acquisition system automatically records the experimental data as well.

### 3 Methodology

To fully understand the change of microstructure characteristics and deformation mechanism of carbonaceous slate during the creep process, X-ray diffraction (XRD), thin section identification, scanning electron microscope and energy dispersion spectrum

(SEM–EDS), mercury intrusion porosimetry (MIP) and triaxial creep test were comprehensively performed. Based on an analysis of carbonaceous slate's mineral composition and microstructure, the creep deformation mechanisms of carbonaceous slate were disclosed by comparing the microscopic information of particle morphology, pore size distribution, and mechanical behaviors before and after creep.

Firstly, SEM–EDS and thin section identification tests were conducted on six cuboid samples and four slides containing carbonaceous slate, respectively. Four to six microregions were selected from each specimen to take six to eight pictures per microregion at 1000–10000 magnification, which were stored at  $2580 \times 1944$  pixel dimensions in RGB format. The mineral grain morphology, texture characteristics, inter-grain pore type, and interstitial distribution were identified by the thin section identification under the orthogonal polarizing microscope and the polarizing microscope for four samples. The surface morphology of the carbonaceous slate section was observed from those images, especially the structure, particle, and microcrack, providing the basis to analyze the mineral composition of carbonaceous slate samples and study the bedding, cleavage, cracks, and mineral arrangement forms of carbonaceous slate before the creep test. The pore size distribution data of the samples were obtained through MIP. Those test results can provide a theoretical basis for microstructure and rheological mechanism analysis. Since those are conventional block material tests, the specific test procedures will not be elaborated.

Secondly, the horizontal and vertical specimens were distinguished and saturated with water in a vacuum at  $-100$  kPa for 48 h. The saturated samples were prepared on GCTS RTX-1000 under the same test conditions with a room temperature of  $20 \pm 0.5$   $^{\circ}\text{C}$ . As there are many research achievements about rock creep at different stress levels and different durations, the study focused on the microstructural changes and mechanism of the creep process with large stress increments and a shorter creep time. Before the creep tests, the sample was placed on the base with the plug installed at the top and then covered with black heat shrink film, which was baked to wrap around the specimen tightly with a hot air blower. Then, the transducers were fixed in the appropriate positions, and the pressure chamber was installed well-sealed and filled with silicone



oil. The creep tests started after setting the initial parameters correctly. A stepwise creep process was executed. The confining pressure was loaded to 6 MPa, and then the deviatoric stress was applied. 10 MPa incremented the vertical specimen at each stage. The stress increment of the horizontal specimen changed to 5 MPa from the third level onwards. The constant stress levels were maintained for a certain time, and the axial and radial strains were measured. The creep duration was 15 h for the first stage, 24 h for both the second and third stages, and 30 h for all subsequent phases until the rock samples failed. The pressures were unloaded, and the creep test ended. Finally, three small samples, each processed from the appropriate locations of the vertical and horizontal damaged creep samples, were again processed. SEM and MIP were performed under the same test conditions for surface morphology and pore characterization.

## 4 Results and discussion

### 4.1 Mineral composition and microstructure

The carbonaceous slate is formed by the slight metamorphism of clayey sedimentary rocks at low temperatures in the region. It is a dark gray bedding

structure enriched with silky and lustrous sericite at the local bedding surface. The microscopic analysis from the X-ray diffraction method, SEM–EDS, and thin section analysis indicated that the slate samples were mainly composed of quartz, sericite, kaolinite, and other clay minerals, and the contents and distribution were uneven (Yang et al. 2023). The orthogonally polarized images collected showed prominent physical characteristics, such as distinct interference colors, texture features, apparent edges between different grains, and clear pore spaces, as seen in Fig. 2.

The carbonaceous slate, having a layered structure, consists mainly of black carbonaceous and clay minerals such as kaolinite, a small amount of granular quartz, and directionally distributed platy sericite. The extrusion of mineral grains under geological action during the rock formation process forms the formation of a bedding microstructure by directional accumulation along its long axis, as seen in Fig. 2a–c, which shows the orientation of the particles along the long axis. The accumulation direction of flaky particles is consistent with the bedding plane. Figure 2d, e show the particle distribution of minerals. The granular quartz had no apparent decomposition, very fine scale-like mica formed lamellar clusters, and abundant clay minerals distributed around the grains and clusters. The mica clusters are varied in size, and the fine grain size of quartz and mica is from few to more

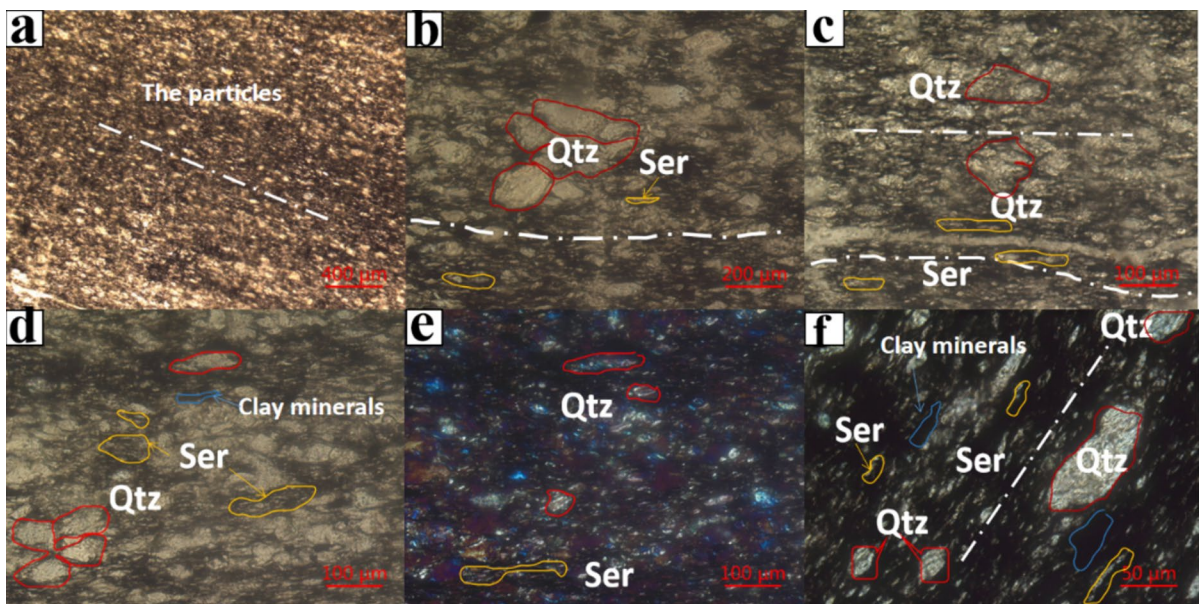


**Fig. 2** Microstructure of carbonaceous slate samples before the creep. Note: Qtz=Quartz, Ser=sericite

than 200  $\mu\text{m}$ , see Fig. 2f. The metamorphic minerals and particles between the layers are well-cemented. It is well known that the material of the laminate structure has different stress deformation in the horizontal and vertical directions. Studying the composition and structure of carbonaceous slate can provide a basis for analyzing the changes in microstructural characteristics during creep.

#### 4.2 Analysis of surface morphological characteristics

High-resolution micrographs from SEM imaging (in Fig. 3) exhibit surface morphological features, including particle geometry and microfracture distribution. Before the triaxial compression creep test, the carbonaceous slate samples were relatively compact and showed a well-developed parallel foliation with chaotic-aligned microliths on the surfaces. Outlines of clast and widths of the micropores were apparent. The directional arrangement of the plate-like clusters formed by the lamellar grains constitutes a remarkable lamellar structure with fish-scale mineral particles with sharp angles and significant interlayer

micro-porosity and microfractures intersecting them. However, during triaxial compression creep, the microscopic morphology of the rock sample underwent significant changes. The tiny particles were subjected to misalignment, dislodging, and migration, partly accumulating to the tips of micro-pores and micro-fractures with time under the combined action of stress and water. Therefore, the particle clusters had rounded edges, blunted microfracture angular tips, and protruding particles such as quartz.

The surface morphology, particle edge, and fracture geometry have changed greatly from before creep (Fig. 3a–c) to after creep (Fig. 3a1–c1). It concluded that creep is the process of realignment between microscopic particles and microfractures of the material in the rock mass under stress and that this process is characterized by time-dependent deformation.

#### 4.3 Pore size and distribution characteristics

MIP experiment is an effective way to study pore body characteristics and has been widely applied to

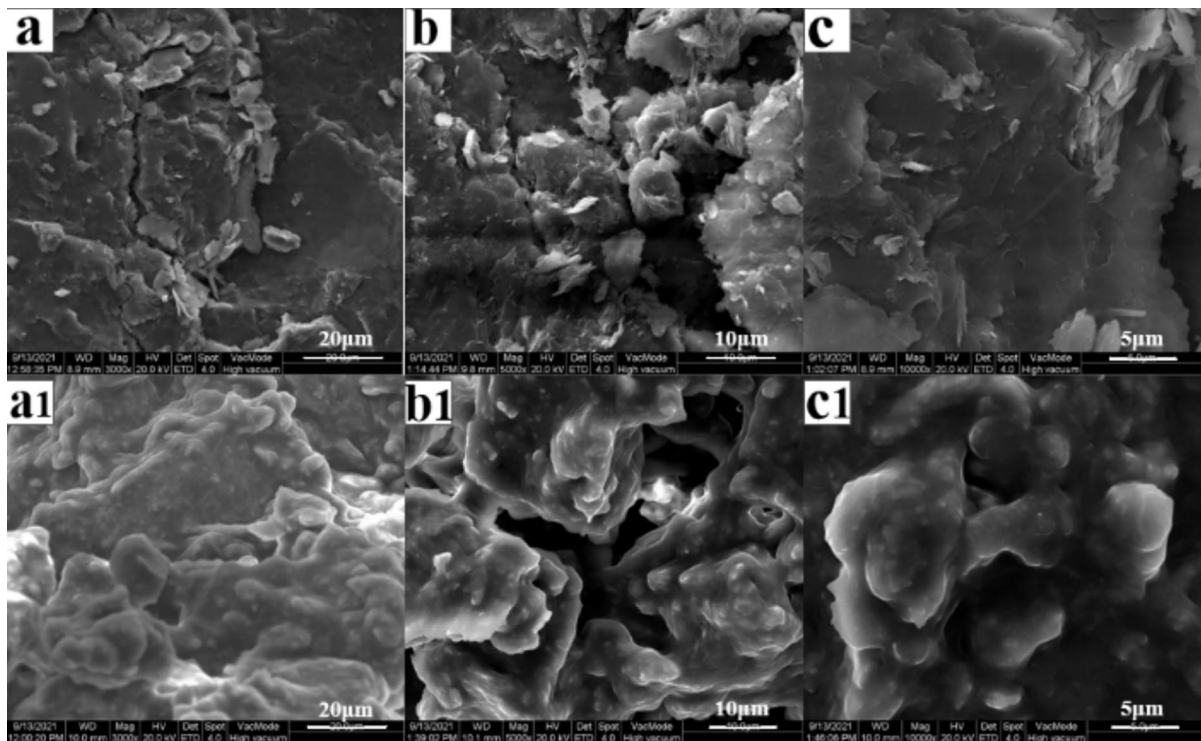


**Fig. 3** Comparison of the surface morphology

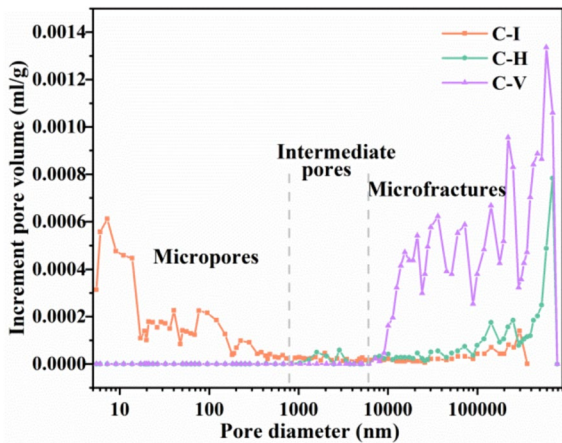


Fig. 4 The changes in pore size distribution

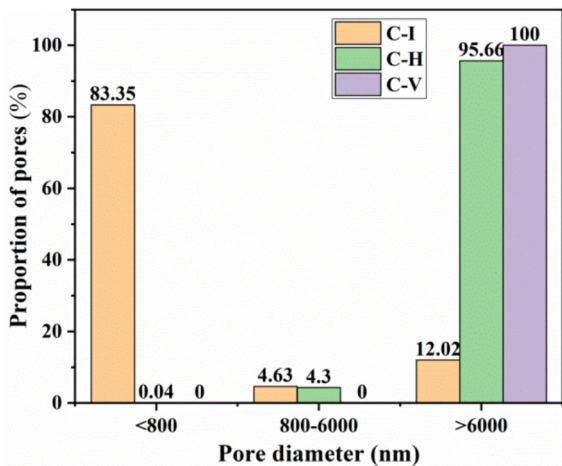


Fig. 5 Pore proportion at different pore sizes

determine the pore size distribution (Li et al. 2018). The specimen before the creep test was recorded as C-I, and the horizontal and vertical creep samples were marked as C-H and C-V, respectively. The pore volume and relative proportion with diameter

for the three samples obtained from MIP experiments are shown in Figs. 4 and 5, respectively. Those less than 800 nm were called micro-pores, those greater than 6000 nm were called micro-fractures, and pores between them were called intermediate pores. By comparing the test data, the pores of the initial specimens before the creep test mainly consisted of micro-pores less than 1 μm and micro-fractures larger than 100 μm, with the former accounting for 83.35% and the latter accounting for 12.02%. However, the number of micropores of the horizontal and vertical samples after creep was 0, and the micro-fractures larger than 50 μm were dominant. The percentage of micro-fractures and intermediate pores in horizontal specimens was 95.7% and 4.3%, respectively. In comparison, the pores in vertical samples were microfractures (accounting for 100%). The volume of microcracks in vertical specimens was much more than that in the horizontals. Based on the previous analyses of the composition, microstructure, and surface morphology of the carbonaceous slate, the transformation of all micropores into cracks can be explained as follows: under stress, the compression of the lamellar particles led to the closure of the intergranular micropores, and very fine particles broken off from the lamellae were filled and deposited within the voids at the tips of the microfractures. It caused microcracks to disappear and microfractures to increase after the specimens underwent the creeping process.

During triaxial compression creep, the pore size distribution of the rock sample changed, leading to the variation in bulk density, as seen in Table 1. The porosity of the C-I was 2.011%, which was more significant than that of the C-H (1.1402%) and smaller than that of the C-V (4.8738%) after creep. The total pore volumes had the same variation trend, while the bulk density changed just the opposite. It indicates that the horizontal specimens underwent irrecoverable pressure dissolution of some lamellar particles and the closure of intergranular micropores due

Table 1 The changes in some physical parameters of specimens

Samples ID	Mass (g)	Volume (mL)	Volume density (g/mL)	Porosity (%)	Total pore volume (mL/g)
C-I	3.5970	1.3773	2.6117	2.0110	0.0077
C-H	4.2001	1.5472	2.7147	1.1402	0.0042
C-V	3.3578	1.3159	2.5517	4.8738	0.0191



to compression caused by the stress on the vertical lamellar surface. Hence, the porosity is smaller, and the compactness is greater. In contrast, the interlayer cement of the vertical specimen was dislocated and damaged due to the stress parallel to the lamellar particles, forming multiple columnar units (see Fig. 9b), and the tensile cracks between the columnar units were further extended, resulting in an increase in porosity and a decrease in bulk density.

#### 4.4 Creep deformation characteristics and mechanism analysis

To compare and analyze the different deformations of horizontal and vertical samples before and after creep, the same confining pressure, durations, and stress increments in the first two stages were maintained during the triaxial compression creep experiments. The relationship of the layered planes with the stresses in the 3D orthogonal coordinate is shown in Fig. 6. The relationships between stress and strain are as follows:

$$\sigma_c = \sigma_2 = \sigma_3 \quad (1)$$

$$\sigma_d = \sigma_1 - \sigma_3 \quad (2)$$

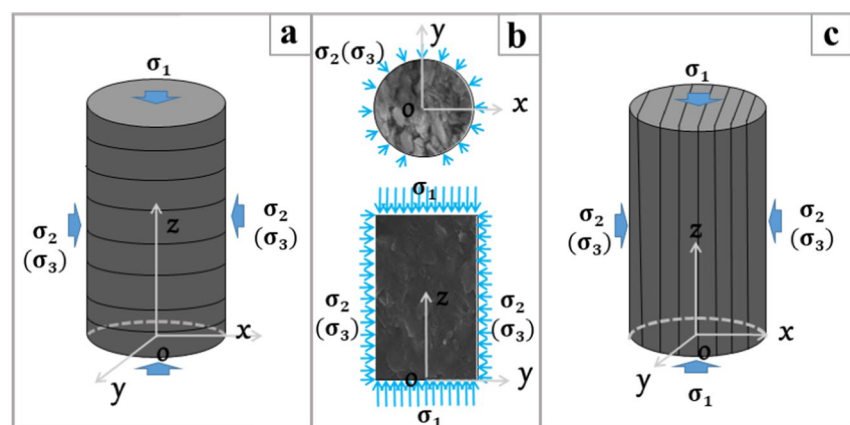
$$\varepsilon_v = \varepsilon_1 + \varepsilon_2 + \varepsilon_3 = \varepsilon_1 + 2\varepsilon_3 \quad (3)$$

$$E_0 = \frac{\Delta\sigma}{\Delta\varepsilon} \quad (4)$$

where  $\sigma_1$  represents axial stress;  $\sigma_2, \sigma_3$  represent the radial stress,  $\sigma_c$  and  $\sigma_d$  represent the confining stress and the deviatoric stress, respectively.  $\varepsilon_1$  is the axial strain,  $\varepsilon_2, \varepsilon_3$  are the radial strains and  $\varepsilon_v$  is the volumetric strain. The  $E_0$  is the deformation modulus,  $\Delta\sigma$  and  $\Delta\varepsilon$  are the stress and strain increments, respectively.

In the triaxial compression creep tests, the confining stress was applied first and remained unchanged. And then, the axial pressures were applied continuously to the rock sample until failure. Figure 7 shows the evolution of axial and radial strains with time. After the load was applied, creep strain that decays off swiftly occurred. At a confining pressure of 6 MPa, the vertical sample experienced four creep processes due to its more considerable strength and finally failed in the next stage of loading with the maximum stress of 47 MPa and the max volumetric strain of 0.47% at the time of failure, while the horizontal sample underwent only two complete creep processes and was failed shortly after the third stage of loading with the stress of 25 MPa and the axial strain of 1.28% at the time of failure. Each phase showed different forms of creep due to diverse stress levels, and strain processes varied considerably. To further study the deformation mechanism from microscopic structure, the deformation behaviors were researched during both the transient loading and the creep processes. In the instantaneous loading process, the radial confining pressure was firstly exerted to 6 MPa with the deviatoric stress fluctuating from 0 to  $-0.9$  MPa. The deviatoric stress increment of 10 MPa was applied in

**Fig. 6** Schematic representation of the forces on the rock samples. **a** The horizontal sample. **b** Sectional view of rock samples. **c** The vertical sample



(a) The horizontal sample. (b) Sectional view of rock samples. (c) The vertical sample.



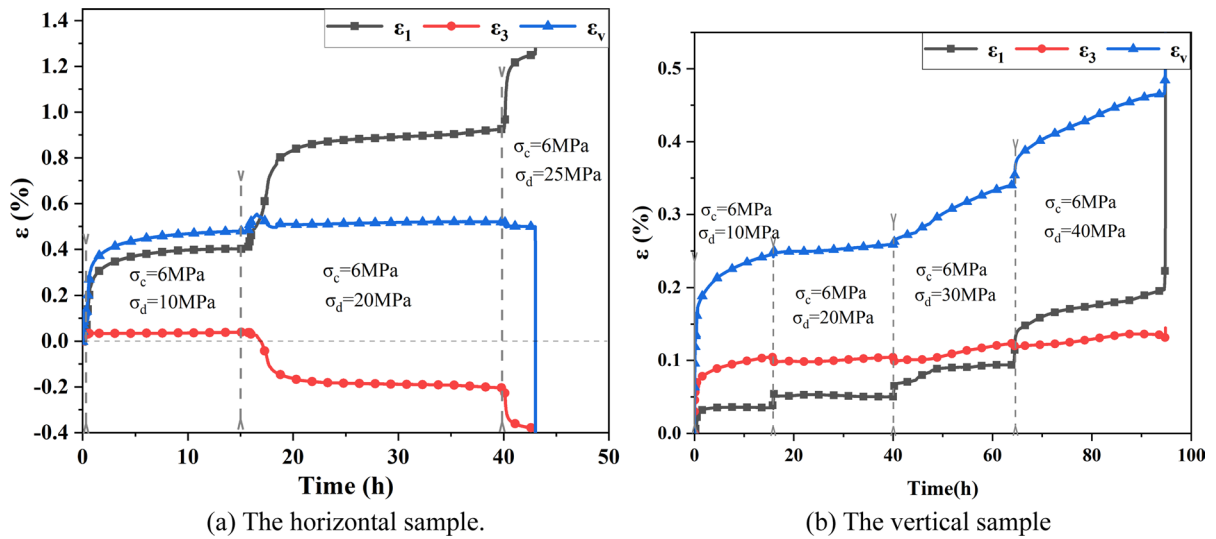


**Fig. 7** The strains' variation with time during the creep processes. **a** The horizontal sample. **b** The vertical sample

the first two stages. Then, the increment value of the horizontal sample changed to 5 MPa, and that of the verticals remained unchanged until the failure. The stress–strain relationships are shown in Fig. 8.

In applying confining pressure, the axial strains of the horizontal sample showed a similar trend to the radial strains of the verticals, which were about 0.068% and 0.064%, respectively. It revealed that the rock samples were in a three-dimensional compression state, so the volume strains were less affected by the bedding angle, which was about 0.13%. The results of volumetric deformation were the compression of the micropores among the plate-like particles in the normal direction.

The deformations of the horizontal sample at the early stages of deviatoric stress application were dominated by the linear increased axial strain. The axial transient strain at the stress level of 52% was 0.22%, and the axial creep strain increment was 0.18%. During the continued increase of the axial stress to a stress level of 84%, the axial transient strain still increased linearly, while the deformation modulus was slightly increased than that of the previous loading stage, and the axial strains increased from 0.40% to 0.47%. However, the radial transient strain and creep strain values were almost constant during the above process. At a stress level of 80%, the axial creep increment of the rock sample was 0.46%, while the radial strain changed from 0.029 to −0.20%, and

the axial and radial strain increments were larger in the subsequent stages until the rock sample failed. Due to the flaky particles torn and/or cement among the layers broken, the fracture surfaces penetrated the horizontal bedding plane and connected with the broken bedding planes, and the sample failed (see Fig. 9a). However, the deformation of the vertical sample was different from that of the horizontals. With the deviatoric stress level increase from 0 to 68%, the axial transient strain increased linearly with an incremental value of 0.07%, and almost no radial transient deformation occurred. The axial creep values during stress levels of 30% and 49% were nearly zero, while the amount of radial creep was 0.03% and 0.006%, respectively. It is inferred that the densities of the rock samples almost reached their maximum values after the previous loading and creep phases. The axial creep strain value at the stress level of 68% increased with an increment of 0.027%, which indicated that the sample fractured. The radial creep strains remained rising, and it seems that the sample could be further compressed. The picture of the destruction of the vertical sample in Fig. 9b presents a reasonable explanation. It demonstrated that transverse expansion occurred at the bottom of the specimen, and its deformation could not be measured by the chain sensor located in the middle. It also indicated that the pressure dissolution occurred and some fine particles transferred downward.

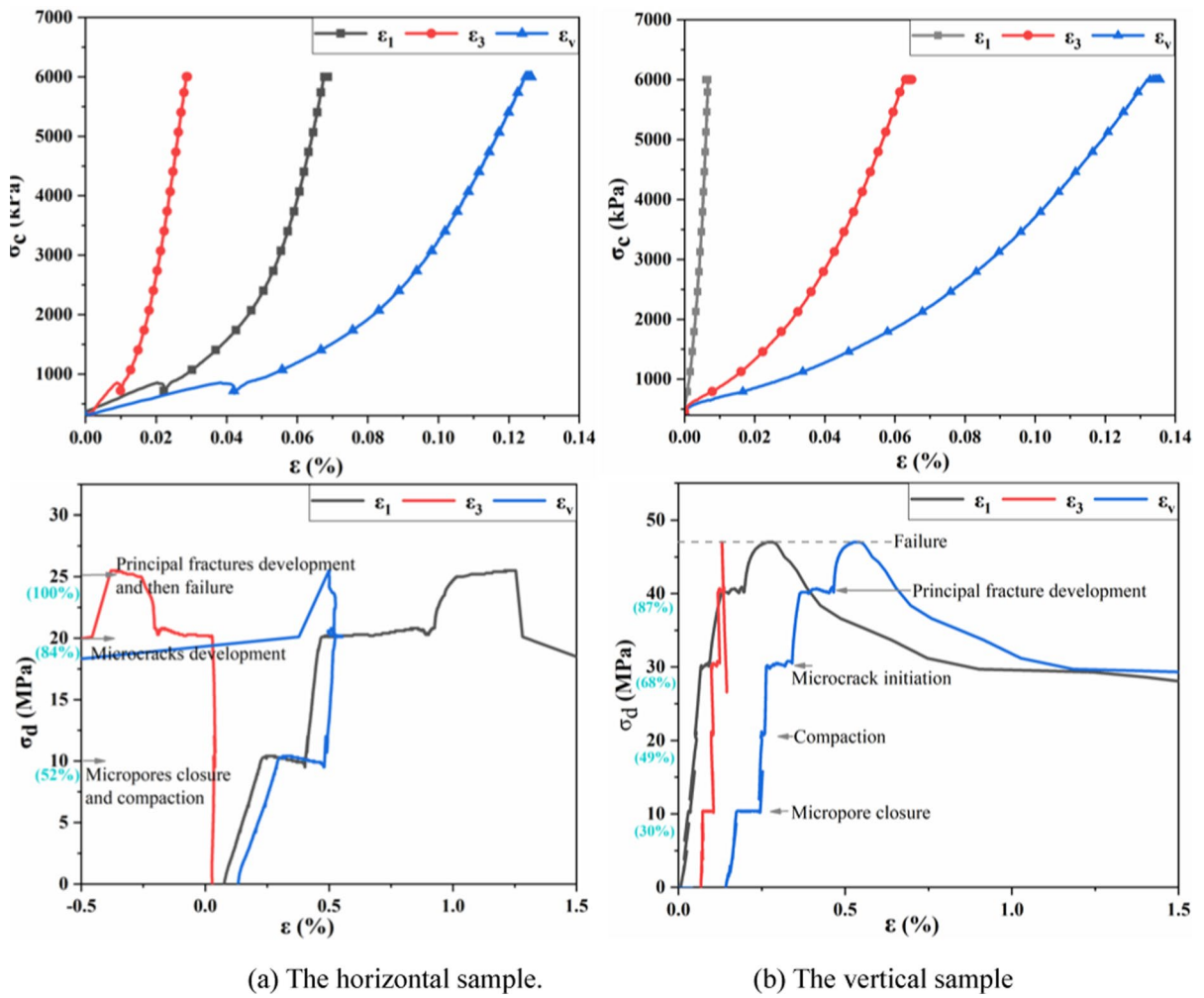
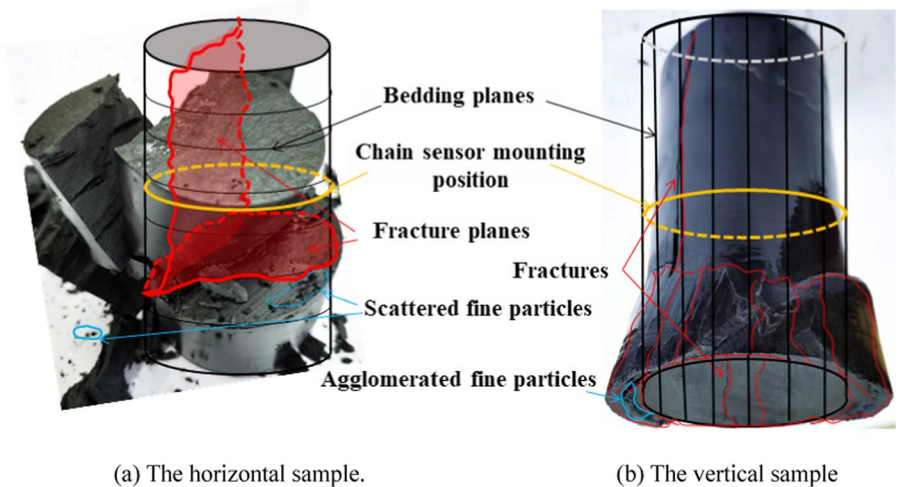


**Fig. 8** The strain–stress relationships of horizontal and vertical specimens. **a** The horizontal sample. **b** The vertical sample

**Fig. 9** Failure patterns of samples after the creep test. **a** The horizontal sample. **b** The vertical sample



From the above microscopic analysis, it was inferred that the flaky particles of the rock sample underwent bending and compression deformation under stresses parallel and perpendicular to their planes, resulting in different creep behaviors of the layered sample in the two directions. The microporosity closure between the particle clusters was the main reason for triaxial compression creep at low stress levels, which was a time-dependent process. As deviatoric stress increased, the porosity of the sample diminished, and the compactness and the deformation modulus accordingly enlarged, making the deformation smaller. The inter-laminar cement breakage or particle tearing under high-stress levels and constantly generating fractures and further expansion resulted in the deformations. This process was accompanied by pressure dissolution and partial migration of very fine particles, so creep deformation was remarkable and lasted for a long time.

In order to further analyze the time dependence of the deformation, the creep phase curves are obtained

by removing the loading phase strain from the above data, see Fig. 10. The graphs of the vertical and horizontal samples were smooth without fluctuation, indicating that the creep deformation has good continuity with time. In Fig. 10a, the curves of the horizontal sample at different stress levels showed apparent primary and secondary creeps and did not show noticeable tertiary creep before failure. The transient creep with rapid strain increment caused by the loading lasted for a shorter time, while the steady creep at a low or nearly constant strain rate persisted for longer. With the increase of the axial compressive stress, the strain rate was reduced rapidly from large to small and finally remained nearly constant. At 10 MPa deviatoric stress, the volumetric strain was governed by axial strain. During the 15 h, the axial creep of 0.1779% is much larger than the radial creep (0.0052%), which indicates that the creep deformation of the rock sample at this stage originated from the closure of micro-pores and micro-fractures between the lamellar particles, and the particle skeleton was

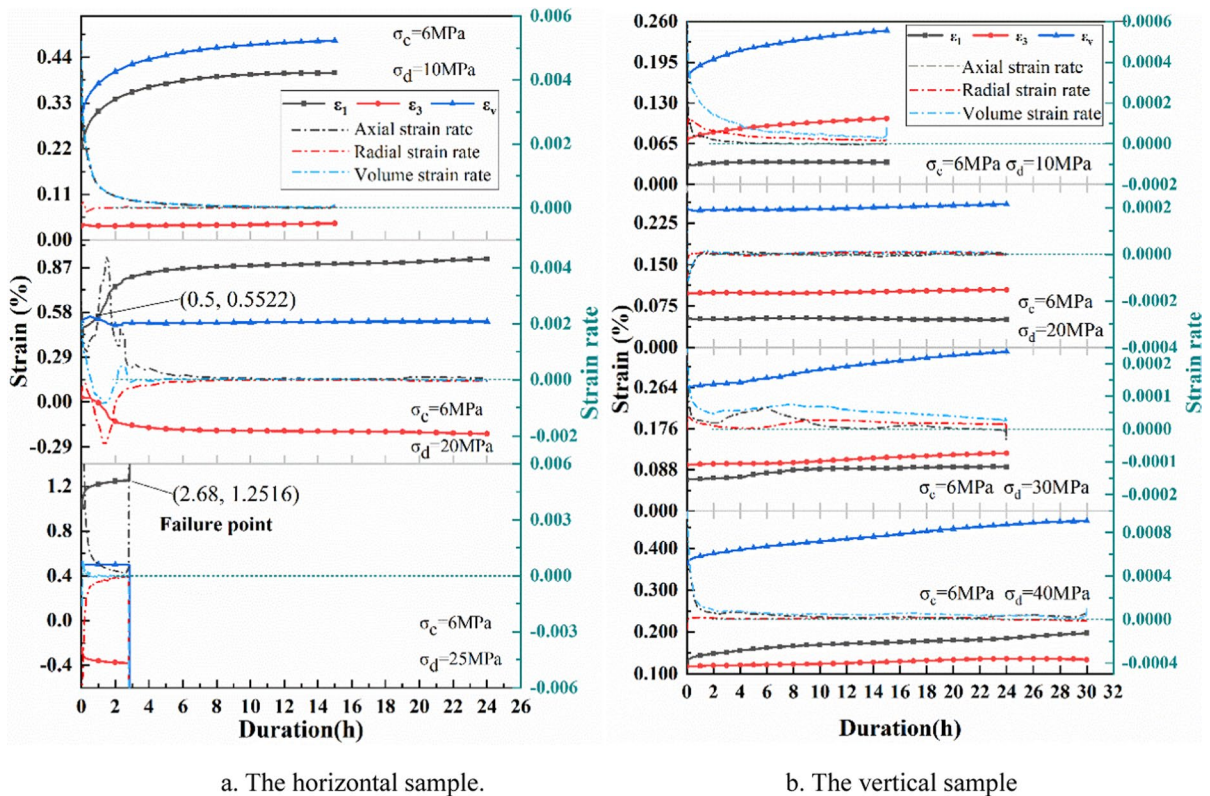


**Fig. 10** The strain variations of the samples during creep. **a** The horizontal sample. **b** The vertical sample

not damaged. At 20 MPa deviatoric stress, the radial strain remained constant for a short time and then changed from 0.0289 to  $-0.2047\%$ , while the axial strain increased from 0.467 to 0.926%. Then, the axial and radial strain values increased with a similar trend in opposite directions, so the volumetric strain remained constant. After about 1 h during the creep process, which keeps the stress state constant, the rock sample ruptured along a weak surface, and the particles moved along the radial direction, which showed typical creep characteristics. The rock sample shortens axially and expands radially, so the volumetric strain remains constant. At deviation stress of 25 MPa, the axial and radial strain trends were similar to those of the previous stage, and the volume strain remained constant at around 0.5%. After holding the load for 168 min, brittle failure without significant plastic deformation occurred. It indicated that the rock samples underwent time-dependent deformation in a highly stressed state after loading and compaction. This process can be interpreted from a microscopic point of view as the pressure dissolution of particles at the interface of the rock samples and migration of particles (Akker et al. 2021), which resulted in the formation of microcracks and their continual expansion, causing radial dilatation. However, the strain behaviors of the vertical sample differed significantly from that of the horizontal sample, as seen in Fig. 10b. During the transient creep at a deviatoric stress of 10 MPa, the radial strain was larger than the axial strain, which was 0.0329% and 0.0066%, respectively. The deformation law was just opposite to that of the horizontal sample. Holding the deviator stress of 20 MPa for 24 h, axial and radial strain increments were maintained at 0.0033% and 0.006%, respectively, similar to the instantaneous values after applying axial pressure. It indicates that the rock samples had high density and low porosity in the stationary creep stage. After holding a deviatoric stress of 30 MPa for about 250 min, noticeable axial plastic strain and large strain rate were all noticed from this moment onwards. The axial strain grew persistently for a particular time and then remained stable. In the next loading process, the axial strain exceeded the radial strain and grew until the rock sample failed. It concluded that in the primary creep stage, the amount of radial creep in vertical specimens is significantly greater than the amount of axial creep, and the deformation behavior is just opposite

to that of the horizontal samples at low stress levels. The reasonable explanation is the compression of micropores between lamellar particles due to the bending deformation of the particles. While the particle skeleton was mainly in the elastic stage and did not undergo damage, the creep characteristics were more significant. In the next stage, the rock samples that were compressed to form the maximum density had no significant creep deformation in the duration. When the deviatoric stress gradually increases to a higher level, the particles need some time for stress adjustment, and some of the particles undergo dislocation fracture, or the bond between particles undergoes tensile damage to form shear and tensile cracks, and directional migration occurs to produce fracture interfaces and continuous deformation, and ultimately toughness damage occurs.

To sum up, combined with the analysis of the horizontal and vertical specimens's surface morphology, microporosity and pore size distribution changes, deformation characteristics before and after creep, and the analysis of the damage patterns after the specimens failed, it can be concluded that the microstructural features, the bedding structure is an essential factor affecting the creep behaviors of carbonaceous slate. Horizontally and vertically layered rock samples undergo compression and bending deformation of the particles during the process of axial stress increase, which makes the intergranular micropores compress and close. Significant transient deformation and transient creep occurred after loading at low-stress levels. The strain rate decreased rapidly until the rock entered the steady creep stage, and the strain value changed less during creep in a very dense stage. The high compression stress contributed to the plastic deformation of cementitious material, particle dislocation movement, compressive solution, and redeposition, leading to the internal crack emergence, expansion, and destruction of the samples under high stress. The delayed breakage of some particles was a vital component in the rearrangement of the skeleton over time in the creep (Karimpour and Lade 2013). Pore deformation has a strong time dependence. Whether it was micropore closure or microcrack expansion, it showed the characteristics of significant creep deformation. Creep behavior and damage patterns were distinct for rock samples with different lamina angles. Horizontal samples under axial compressive stresses showed brittle damage with particles tearing



along the weakened surfaces. However, the vertical sample was subject to shear damage due to bonding between particles, forming multiple penetrating breakages along the laminae surface and transforming the rock samples into multiple columnar joint carriers. It underwent great plastic deformation under the high confining pressure, thus showing ductile damage. Once the pressure was removed, the sample was split along the direction of the slaty cleavage, weakening its resistance to external stress. Among them, the stacking direction and stress direction of lamellar particles had a great influence on the volumetric deformation of the rock sample.

## 5 Conclusion

In order to uncover the macroscale creep properties and the deformation mechanisms of the carbonaceous slate, microstructural and triaxial compression creep tests were performed to obtain particle shape, surface morphology, microstructure attributes, and the time-dependent creep behaviors of the vertical and horizontal samples. The comparison of the microstructure and the measured strains before and after creeps were analyzed, and the conclusions are as follows:

- (1) Carbonaceous slate is a low-grade metamorphic, layered rock mass. In the deposition process, inter-particle micropores and intersecting microcracks form in a complex diagenetic process. During triaxial compression, microcracks between particles of a saturated specimen are closed at low stress. At low stress levels, the rock specimen becomes dense, and as the stress continues to increase, the macroscopic shear and tension cracks in the specimen continue to expand and increase in number, and damage occurs. Under the same confining pressure, the horizontal specimens showed brittle damage, while the vertical specimens showed ductile damage.
- (2) The lamellar microporosity between particles has an important influence on the creep mechanical behavior of rock specimens. Due to the presence of intergranular microporosity, lamellar particles produce compressive or bending strains that are several times higher than those in the other two directions, and the gap between these different directional deformations decreases with increasing compactness. When the stress is perpendicular to the laminae, creep deformation is caused by the destruction of the grains at the maximum compressive stress, whereas when the stress is parallel to the laminae surface, cracks are formed due to the shear destruction of the cement between the grains with further dislocation of the very fine grains.
- (3) Creep deformation of carbonaceous slate is mainly manifested in the stage of significant changes in porosity, with a high time dependence. Whether in the stage of microporosity closure or microfissure expansion, the creep deformation is large and long-lasting, while in the stage of maximum densification, the creep deformation is small. The specimen generated rupture surfaces under high stress, very fine particles underwent pressure dissolution, misalignment, and migration, and micropores were either compacted or filled, which made the intergranular microfractures of the saturated specimen disappear and the number of microfractures increases. Those conclusions reasonably explain that the tunnel surrounding the rock body is prone to creep failure damage in the local area where the laminar inclination angle has been changed sharply. It also provides a basis for the creep ontological relationship of carbonaceous slate and its parameter optimization.

**Acknowledgements** The authors gratefully acknowledge the financial support provided by the National Natural Science Foundation of China (Grant No.41831286).

**Author Contribution** All authors participated in the study and their contributions were as follows: Hucheng Yang (First author) completed the creep tests, the analysis of the test data, and the writing of the manuscript; Peng Li conducted the experimental method design and data management; Shengrui Su reviewed and revised the manuscript; Jianxun Chen is mainly responsible for the supervision of research projects.

**Funding** The research leading to these results received funding from the National Natural Science Foundation of China under Grant Agreement No. 41831286.

**Data availability** Some or all data generated or used during the study is available from the corresponding author upon reasonable request.

## Declarations

**Competing interests** The authors declare no competing interests.

**Ethics approval** All authors declared that the submitted manuscript was original and did not be published and submitted to more than one journal. The experimental data in this manuscript was real and accurate, the study conclusions were clear, and the research methods were scientific. There is no potential conflict of interest regarding the manuscript.

**Consent to publish** All authors agreed with the content, and they gave explicit consent to submit and obtained consent from the responsible person before the work was submitted.

**Conflict of interest** The authors certify that they have no affiliations with or involvement in any organization or entity with any financial interest or non-financial interest in the subject matter or materials discussed in this manuscript.

**Open Access** This article is licensed under a Creative Commons Attribution 4.0 International License, which permits use, sharing, adaptation, distribution and reproduction in any medium or format, as long as you give appropriate credit to the original author(s) and the source, provide a link to the Creative Commons licence, and indicate if changes were made. The images or other third party material in this article are included in the article's Creative Commons licence, unless indicated otherwise in a credit line to the material. If material is not included in the article's Creative Commons licence and your intended use is not permitted by statutory regulation or exceeds the permitted use, you will need to obtain permission directly from the copyright holder. To view a copy of this licence, visit <http://creativecommons.org/licenses/by/4.0/>.

## References

- Akker IV, Berger A, Schrank CE, Jones MWM, Kewish CM, Klaver J, Herwegh M (2021) The evolution of slate microfabrics during progressive accretion of foreland basin sediments. *J Struct Geol* 150:104404. <https://doi.org/10.1016/j.jsg.2021.104404>
- Barla G, Debernardi D, Sterpi D (2012) Time-dependent modeling of tunnels in squeezing conditions. *Int J Geomech* 12(6):697–710. [https://doi.org/10.1061/\(ASCE\)GM.1943-5622.0000163](https://doi.org/10.1061/(ASCE)GM.1943-5622.0000163)
- Boukharov GN, Chanda MW, Boukharov NG (1995) The three processes of brittle crystalline rock creep. *Int J Rock Mech Min Sci Geomech* 32(4):325–335. [https://doi.org/10.1016/0148-9062\(94\)00048-8](https://doi.org/10.1016/0148-9062(94)00048-8)
- Brzesowsky R, Spiers C, Peach C, Hangx S (2014) Time-independent compaction behavior of quartz sands. *J Geophys Res Solid Earth* 119(2):936–956. <https://doi.org/10.1002/2013JB010444>
- Chen ZM, Zhao D, Yu YY (2011) The interaction mechanism of surrounding rock and supporting structure in high geostress extrusion fault. *Adv Mater Res* 243–249:3588–3598. <https://doi.org/10.4028/www.scientific.net/AMR.243-249.3588>
- Coop M, Sorensen K, Freitas TB, Georgoutsos G (2004) Particle breakage during shearing of a carbonate sand. *Geotechnique* 54(3):157–163. <https://doi.org/10.1680/geot.2004.54.3.157>
- Debernardi D, Barla G (2009) New viscoplastic model for design analysis of tunnels in squeezing conditions. *Rock Mech Rock Eng* 42:259–288. <https://doi.org/10.1007/s00603-009-0174-6>
- Gasc-Barbier M, Chanchole S, Berest P (2004) Creep behavior of Bure clayey rock. *Appl Clay Sci* 26(1/4):449–458. <https://doi.org/10.1016/j.clay.2003.12.030>
- Gunther RM, Salzer K, Popp T, Ludeling C (2015) Steady-state creep of rock salt: improved approaches for lab determination and modeling. *Rock Mech Rock Eng* 48(6):2603–2613. <https://doi.org/10.1007/s00603-015-0839-2>
- Hamza O, Stace R (2018) Creep properties of intact and fractured muddy siltstone. *Int J Rock Mech Min Sci* 106:109–116. <https://doi.org/10.1016/j.ijrmms.2018.03.006>
- Haupt M (1991) A constitutive law for rock salt based on creep and relaxation tests. *Rock Mech Rock Eng* 24(2):179–206. <https://doi.org/10.1007/BF01045031>
- Karimpour H, Lade PV (2013) Creep behavior in Virginia beach sand. *Can Geotech J* 50(11):1159–1178. <https://doi.org/10.1139/cgj-2012-0467>
- Li SC, Hu C, Li LP, Song SG, Zhou Y, Shi SS (2013) Bidirectional construction process mechanics for tunnels in dipping layered formation. *Tunn Undergr Sp Tech* 36:57–65. <https://doi.org/10.1016/j.tust.2013.01.009>
- Li XC, Kang YL, Haghighi M (2018) Investigation of pore size distributions of coals with different structures by nuclear magnetic resonance (NMR) and mercury intrusion porosimetry (MIP). *Measurement* 116:122–128. <https://doi.org/10.1016/j.measurement.2017.10.059>
- Lin JM, Sun J (1993) Mesoscopic crack damage in brittle rocks and its aging characteristics. *Chin J Rock Mech Eng* 12(4):304–312
- Maranini E, Brignoli M (1999) Creep behaviour of a weak rock: experimental characterization. *Int J Rock Mech Min Sci* 36(1):127–138. [https://doi.org/10.1016/S0148-9062\(98\)00171-5](https://doi.org/10.1016/S0148-9062(98)00171-5)
- Pellet FF (2006) Creep and time-dependent damage in argillaceous rocks. *Int J Rock Mech Min Sci* 43(6):950–960. <https://doi.org/10.1016/j.ijrmms.2006.02.004>
- Scholz CH (1968) Mechanism of creep in brittle rock. *J Geophys Res* 73(10):3295–3302. <https://doi.org/10.1029/JB073i010p03295>
- Shao JF, Zhu QZ, Su K (2003) Modeling of creep in rock materials in terms of material degradation. *Comput Geotech* 30(7):549–555. [https://doi.org/10.1016/S0266-352X\(03\)00063-6](https://doi.org/10.1016/S0266-352X(03)00063-6)
- Shi X, Yang X, Meng Y, Gao L (2016) An anisotropic strength model for layered rocks considering planes of weakness. *Rock Mech Rock Eng* 49(9):3783–3792. <https://doi.org/10.1007/s00603-016-0985-1>
- Sone H, Zoback MD (2013) Mechanical properties of shale-gas reservoir rocks—part 2: ductile creep, brittle strength, and their relation to the elastic modulus. *Geophysics*

- 78(5):D393–D402. <https://doi.org/10.1190/GEO2013-0051.1>
- Sterpi D, Gioda G (2009) Visco-plastic behaviour around advancing tunnels in squeezing rock. *Rock Mech Rock Eng* 42:319–339. <https://doi.org/10.1007/s00603-007-0137-8>
- Sun J (2007) Rock rheological mechanics and its advance in engineering application. *Chin J Rock Mech Eng* 26(6):1081–1106
- Tien YM, Kuo MC, Juang CH (2006) An experimental investigation of the failure mechanism of simulated transversely isotropic rocks. *Int J Rock Mech Min Sci* 43(8):1163–1181. <https://doi.org/10.1016/j.ijrmms.2006.03.011>
- Tomanovic Z (2006) Rheological model of soft rock creep based on the tests on marl. *Mech Time-Depend Mat* 10:135–154. <https://doi.org/10.1007/s11043-006-9005-2>
- Wang ZC, Zong Z, Qiao L, Li W (2018a) Elastoplastic model for transversely isotropic rocks. *Int J Geomech* 18(2):04017149. [https://doi.org/10.1061/\(ASCE\)GM.1943-5622.0001070](https://doi.org/10.1061/(ASCE)GM.1943-5622.0001070)
- Wang ZC, Zong Z, Qiao LP, Li W (2018b) Transversely isotropic creep model for rocks. *Int J Geomech* 18(6):04018033. [https://doi.org/10.1061/\(ASCE\)GM.1943-5622.0001159](https://doi.org/10.1061/(ASCE)GM.1943-5622.0001159)
- Xu WY, Yang SQ, Chu WJ (2006) Nonlinear viscoelastic-plastic rheological model (Hohai model) of rock and its engineering application. *Chin J Rock Mech Eng* 25(3):433–447. [https://doi.org/10.1016/S1872-1508\(06\)60035-1](https://doi.org/10.1016/S1872-1508(06)60035-1)
- Yang WD, Zhang QY, Li SC, Wang SG (2014) Time-dependent behavior of diabase and a nonlinear creep model. *Rock Mech Rock Eng* 47:1211–1224. <https://doi.org/10.1007/S00603-013-0478-4>
- Yang HC, Su SR, Li P, Chen JX (2023) Investigation of the microstructure characteristics and deformation mechanisms of the carbonaceous slate under hydromechanical coupling. *Geofluids*. <https://doi.org/10.1155/2023/5490136>
- Zhang YD, Buscarnera G (2017) A rate-dependent breakage model based on the kinetics of crack growth at the grain scale. *Geotechnique* 67(11):953–967. <https://doi.org/10.1680/jgeot.16.P.181>
- Zhang Z, Xu W, Wang W, Wang R (2012) Triaxial creep tests of rock from the compressive zone of dam foundation in xiangjiaba hydropower station. *Int J Rock Mech Min Sci* 50:133–139. <https://doi.org/10.1016/j.ijrmms.2012.01.003>
- Zhang Y, Shao JF, Xu WY, Jia Y, Zhao HB (2015) Creep behaviour and permeability evolution of cataclastic sandstone in triaxial rheological tests. *Eur J Environ Civ Eng* 19(4):496–519. <https://doi.org/10.1080/19648189.2014.960103>
- Zhang YD, Buscarnera G, Einav I (2015b) Grain size dependence of yielding in granular soils interpreted using fracture mechanics, breakage mechanics and Weibull statistics. *Geotechnique* 66(2):1–12. <https://doi.org/10.1680/jgeot.15.P.119>
- Zhang L, Li XC, Gao JX, An ZX, Yang XH, Nie BS (2020) Creep characteristics and constitutive model of coal under triaxial stress and gas pressure. *Energy Sci Eng* 8(2):501–514. <https://doi.org/10.1002/ese3.532>
- Zhao YL, Zhang LY, Asce M, Wang WJ, Wan W, Ma WH (2018) Separation of elastoviscoplastic strain of rock and a nonlinear creep model. *Int J Geomech* 18(1):04017129. [https://doi.org/10.1061/\(ASCE\)GM.1943-5622.0001033](https://doi.org/10.1061/(ASCE)GM.1943-5622.0001033)

**Publisher's Note** Springer Nature remains neutral with regard to jurisdictional claims in published maps and institutional affiliations.